SIAM J. SCI. COMPUT.
Vol. 28, No. 1, pp. 382–402

AN ADAPTIVE HYBRID FEM/FDM METHOD FOR AN INVERSE SCATTERING PROBLEM IN SCANNING ACOUSTIC MICROSCOPY*

LARISA BEILINA† AND CHRISTIAN CLASON‡

Abstract. Scanning acoustic microscopy based on focused ultrasound waves is a promising new tool in medical imaging. In this work we apply an adaptive hybrid FEM/FDM (finite element methods/finite difference methods) method to an inverse scattering problem for the time-dependent acoustic wave equation, where one seeks to reconstruct an unknown sound velocity $c(x)$ from a single measurement of wave-reflection data on a small part of the boundary, e.g., to detect pathological defects in bone. Typically, this corresponds to identifying an unknown object (scatterer) in a surrounding homogeneous medium.

The inverse problem is formulated as an optimal control problem, where we use an adjoint method to solve the equations of optimality expressing stationarity of an associated augmented Lagrangian by a quasi-Newton method. To treat the problem of multiple minima of the objective function, the optimization procedure is first performed on a coarse grid to smooth the high frequency error, generating a starting point for optimization steps on successively refined meshes. Local refinement based on the results of previous steps will improve computational efficiency of the method.

As the main result then, an a posteriori error estimate is proved for the error in the Lagrangian, and a corresponding adaptive method is formulated, where the finite element mesh is refined from residual feedback. The performance of the adaptive hybrid method and the usefulness of the a posteriori error estimator for problems with limited boundary data are illustrated in three dimensional numerical examples.

Key words. inverse scattering, parameter identification, a posteriori error estimator, adaptive mesh refinement, transient wave equation, hybrid finite element/difference method

AMS subject classifications. 65M32, 65M50

DOI. 10.1137/050631252

1. Introduction.

Inverse scattering is a rapidly expanding area of computational mathematics with a wide range of applications including nondestructive testing of materials, shape reconstruction, nonmicroscopic ultrasound imaging, subsurface depth imaging of geological structures, and seismic prospection. The current work is devoted to an adaptive hybrid finite element/difference method (FEM/FDM) for an inverse scattering problem for the time-dependent three dimensional acoustic wave equation, with a special focus on the application of scanning acoustic microscopy (cf. [12]) in medical imaging. This problem takes the form of reconstructing a parameter from a single set of boundary displacement data measured using acoustic microscopy. Since the shear component of the elastic wave speed is much less than the longitudinal component in biological materials (by several orders of magnitude for soft tissue), an approximate common mathematical model for the displacement in water and sample is a scalar wave equation with (longitudinal) wave speed $c = \sqrt{(\lambda + 2\mu)/\rho}$, where ρ is the density and λ, μ are the Lamé constants of linear elasticity. More precisely, we will consider the problem of obtaining quantitative

*Received by the editors May 11, 2005; accepted for publication (in revised form) August 16, 2005; published electronically March 24, 2006.

http://www.siam.org/journals/sisc/28-1/63125.html

†Department of Mathematics, University of Basel, CH–4051 Basel, Switzerland (Larisa.Beilina@unibas.ch). The work of this author was supported by Swiss National Foundation grant 200020-105135.

‡Department of Mathematics, Technische Universität München, D–85748 Garching bei München, Germany (clason@ma.tum.de).

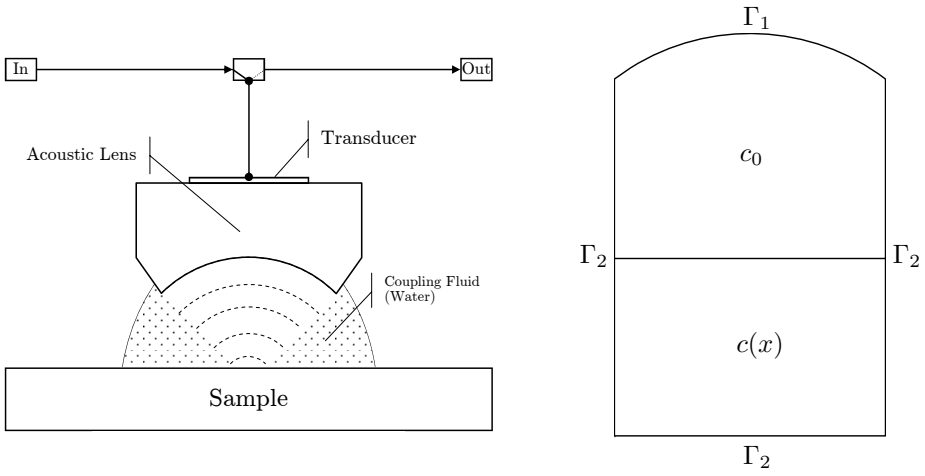

FIG. 1.1. *Sketch of a scanning acoustic microscope (left) and a cut of the corresponding three dimensional computational domain (right). Here,* c_0 *corresponds to the region filled with water,* $c(x)$ *to the sample, and* Γ_1 *to the lens boundary where a pulse is initiated and reflected echoes are measured.*

elasto-mechanical parameters of human bone by identifying the coefficient $c(x)$ in a bounded domain $\Omega \subset \mathbb{R}^3$, where short acoustic impulses are emitted on a part of the boundary $\Gamma_1 \subset \partial\Omega$, which are backscattered by material inhomogeneities and recorded again on Γ_1 (cf. Figure 1.1). In scanning acoustic microscopy, as in many other applications, Γ_1 is only a small part of the boundary, which introduces special difficulties for the reconstruction. Note that this problem differs significantly from another problem often considered in inverse scattering: that of reconstructing internal boundaries from far field measurements (cf. [16]).

Much research has been done to identify a coefficient in a three dimensional hyperbolic equation from boundary measurements. However, most previous papers treat the determination of the coefficient in the zeroth-order part of the hyperbolic operator—see, for example, Romanov [39] (using linearization), Imanuvilov and Yamamoto [25], Puel and Yamamoto [37], Feng et al. [22], and Rakesh [38] (requiring knowledge of the Dirichlet-to-Neumann map). The method of Carleman estimates introduced by Bukhgeim and Klibanov in [13] can prove the uniqueness and the conditional stability by a finite number of observations (cf. [26, 29] and the literature cited there). However, in the method of Carleman estimates it is necessary to assume that initial or external forces should satisfy positivity conditions, which restrict many practical applications.

Without such an assumption the problem of uniqueness and stability is still open. More generally, Bardos, Lebeau, and Rauch [2], using microlocal analysis, justified the rays of geometrical optics as tools for characterizing the stability of controllability for arbitrary domains. Their main result is the (nearly sharp) condition that every such ray must meet the controlled boundary in at least one nonglancing point.

There are different methods for computing the solution of the inverse problem for the acoustic wave equation in the time-domain—see, for example, [11, 40, 46]. Shirota [41] investigated a variational method for the reconstruction of the coefficient in an acoustic wave equation, which gave reasonable reconstruction for a set of given Cauchy data on most of the boundary. But the quality of the reconstruction deteriorated when

the measurement boundary was restricted, limiting the use for cases such as acoustic microscopy.

In order to reconstruct the parameter in a stable manner, we use an adjoint method with added Tikhonov regularization. Adjoint methods are well known in optimal control of partial differential equations [30]. They were also developed to solve inverse problems in different areas under the name of the propagation-backpropagation, time reversal, or phase conjugation method (cf. [32, 36, 42] and the literature cited there). The minimization problem is reformulated as the problem of finding a stationary point of a Lagrangian involving a forward wave equation (the state equation), a backward wave equation (the adjoint equation), and an equation expressing that the gradient with respect to the wave speed c vanishes. The optimum is sought in an iterative process solving in each step the forward and backward wave equations and updating the material coefficients by a quasi-Newton method. In Tikhonov regularization (cf. [18, 43, 45]), a small penalty term is added, stabilizing this ill-posed problem. To treat the problem of multiple local minima arising from the high frequency content of the data, we employ an adaptive approach, where we first solve the inverse problem on a coarse grid to smooth the high frequency components of the error, and then successively refine the mesh locally and use the results of previous iterations as an initial guess for a local optimization in order to capture finer details of the solution. Similar to multigrid methods (cf. [1, 14, 15, 35]), this will extend the basin of attraction of the global minimum, while at the same time improving the computational efficiency by the possibility of local refinement. Given the need for fast evaluation in applications like medical imaging and the high resolution possible with acoustic microscopy, the last point is of special importance.

The main contribution of this work therefore is to derive an a posteriori error estimate for the Lagrangian involving the residuals of the state equation, adjoint state equation, and the gradient with respect to the parameter (following [4, 5, 7, 8, 9, 20, 21, 27]) and employ this in an adaptive method where the spatial discretization is refined locally with feedback from the a posteriori error estimator. We present a numerical example showing the effectiveness of the computational inverse scattering in scanning acoustic microscopy using adaptive error control.

Additionally, often the surrounding body is homogeneous, and the material inhomogeneities occupy only a small portion of the body. In such cases the numerical solution of the wave equation is efficiently performed by a hybrid finite element/finite difference method developed in [6, 10], where the finite difference method is used in the structured part and finite elements are used in the unstructured part of the mesh. We exploit the flexibility of mesh refinement and adaptation of the finite element method in a domain including the object, and the efficiency of a structured mesh finite difference method in the surrounding homogeneous domain. The hybrid scheme can be viewed as a finite element scheme on a partially structured mesh which gives a stable coupling of the two methods.

An outline of the work is the following: in section 2 we formulate the inverse scattering problem and give the formulation of the adjoint method, in section 3 we introduce the finite element discretization, in section 4 we present a fully discrete version used in the computations, and in section 5 we describe the optimization by a quasi-Newton method. Section 6 contains the main result of this work: we prove an a posteriori error estimate and formulate an adaptive algorithm for the solution of the inverse problem. In section 7, we present computational results demonstrating the effectiveness of the adaptive finite element/difference method on an inverse scattering problem for scanning acoustic microscopy in three dimensions.

2. The inverse scattering problem. We consider the scalar wave equation in a bounded domain $\Omega \subset \mathbb{R}^3$, with boundary $\Gamma = \Gamma_1 \cup \Gamma_2$:

$$\begin{cases} \alpha \frac{\partial^2 v}{\partial t^2} - \triangle v &= 0, \quad \text{in } \Omega \times (0,T), \\ v(\cdot,0) &= 0, \quad \frac{\partial v}{\partial t}(\cdot,0) = 0, \text{ in } \Omega, \\ \partial_n v\big|_{\Gamma_1} &= v_1, \quad \text{on } \Gamma_1 \times (0,t_1], \\ \partial_n v\big|_{\Gamma_1} &= 0, \quad \text{on } \Gamma_1 \times (t_1,T], \\ \partial_n v\big|_{\Gamma_2} &= 0, \quad \text{on } \Gamma_2 \times [0,T], \end{cases} \tag{2.1}$$

where $v(x,t)$ is the scalar longitudinal displacement in an isotropic medium, t is the time variable, T is a final time, and $\alpha(x) = \frac{1}{c(x)^2}$ with $c(x) = \sqrt{(\lambda(x) + 2\mu(x))/\rho(x)}$ representing the wave speed depending on $x \in \Omega$. We assume that the density $\rho(x)$ and the Lamé coefficients $\lambda(x)$, $\mu(x)$ are strictly positive. The impulse wave $v_1(x,t)$ is initialized at the spherical boundary of the lens Γ_1 and propagated in time $(0,t_1]$ into Ω, which represents the region of investigation by the acoustic microscope (cf. 1.1).

Our goal is to find the coefficient function $\alpha(x)$ which minimizes the quantity

$$E(v,\alpha) = \frac{1}{2}\int_0^T \int_{\Gamma_1} (v - v_{obs})^2 \, dxdt + \frac{1}{2}\gamma \int_\Omega (\alpha - \alpha_0)^2 \, dx, \tag{2.2}$$

over the set $C_M = \{\alpha \in C(\overline{\Omega}) |\ M^{-1} \le \alpha(x) \le M\}$ for a fixed $M > 0$. Here v_{obs} is the observed data on Γ_1, and v (here understood as its trace on Γ) satisfies (2.1), thus depending on α. The second term involving α_0, an initial guess value for α, is a Tikhonov regularization. The choice of the regularization parameter γ is important in order to get a good reconstruction. This value will depend on the quality of the measured data, with poor data typically demanding more regularization. Several parameter choice rules exist if the noise level is known explicitly, which can be shown to be optimal (cf. [44] and literature cited there). The case of stochastic noise is discussed in [28]. Unfortunately, the noise level is hard to estimate a priori in our application, since it depends strongly on the operating conditions of the microscope and the specific sample to be measured. However, in [9], it was shown that γ can be chosen adaptively to get a best reconstruction by computing stability factors appearing in the solution to a dual linearized problem involving the Hessian of the Lagrangian. In our future research, we plan to study the behavior of the a posteriori error estimator connected to the Hessian problem for the application in scanning acoustic microscopy.

To solve this minimization problem with an adjoint method, we consider the augmented Lagrangian

$$L(u) = E(v,\alpha) + \int_0^T \int_\Omega \left(-\alpha \frac{\partial \lambda}{\partial t}\frac{\partial v}{\partial t} + \nabla\lambda\nabla v \right) \, dxdt - \int_0^{t_1}\int_{\Gamma_1} v_1 \lambda \, d\Gamma dt, \tag{2.3}$$

where $u = (v,\lambda,\alpha)$, and search for a stationary point with respect to u satisfying for all $\bar{u} = (\bar{v},\bar{\lambda},\bar{\alpha})$

$$L'(u)(\bar{u}) = 0, \tag{2.4}$$

where L' is the gradient of L. Equation (2.4) expresses that for all $\bar{u}$,

$$0 = \frac{\partial L}{\partial \lambda}(u)(\bar{\lambda}) = \int_0^T \int_\Omega \left(-\alpha \frac{\partial \bar{\lambda}}{\partial t}\frac{\partial v}{\partial t} + \nabla\bar{\lambda}\nabla v \right) \, dxdt - \int_0^{t_1}\int_{\Gamma_1} v_1 \bar{\lambda} \, d\Gamma dt, \tag{2.5}$$

(2.6)
$$0 = \frac{\partial L}{\partial v}(u)(\bar{v}) = \int_0^T \int_{\Gamma_1} (v - v_{obs})\ \bar{v}\ dxdt + \int_0^T \int_\Omega \left(-\alpha \frac{\partial \lambda}{\partial t} \frac{\partial \bar{v}}{\partial t} + \nabla \lambda \nabla \bar{v} \right)\ dxdt,$$

(2.7)
$$0 = \frac{\partial L}{\partial \alpha}(u)(\bar{\alpha}) = -\int_0^T \int_\Omega \frac{\partial \lambda(x,t)}{\partial t} \frac{\partial v(x,t)}{\partial t} \bar{\alpha}\ dxdt + \gamma \int_\Omega (\alpha - \alpha_0)\bar{\alpha}\ dx, \qquad x \in \Omega.$$

The equation (2.5) is a weak form of the state equation (2.1); (2.6) is a weak form of the adjoint state equation (which is solved backward in time)

(2.8)
$$\begin{cases} \alpha \frac{\partial^2 \lambda}{\partial t^2} - \triangle \lambda & = 0,\ x \in \Omega,\ 0 < t < T, \\ \lambda(\cdot, T) & = \frac{\partial \lambda(\cdot, T)}{\partial t} = 0, \\ \partial_n \lambda & = (v - v_{obs}) \quad \text{on } \Gamma \times [0,T], \end{cases}$$

and (2.7) expresses stationarity with respect to α. From standard results in optimal control theory (e.g., Chapter IV, Lemma 7.1 in [30]), we know that the solution of (2.8) exists and is unique.

The existence of minimizers of (2.2) can be proven using the techniques in [22]. Assuming compatibility conditions for v_1, one can prove a priori estimates in $H^1(\Omega \times [0,T])$ for the gradient of v (cf. [24,31]). Taking a minimizing sequence α_n of (2.2) in C_M with $\lim_{n\to\infty} E(v(\alpha_n), \alpha_n) = \inf_{\alpha \in C_M} E(v(\alpha), \alpha)$ and denoting $v_n = v(\alpha_n)$, we have from the strong convergence of ∇v_n in $L^2(\Omega \times [0,T])$ and the boundedness of α_n^{-1} the convergence of $\alpha_n^{-1} \nabla v_n$ in $L^2(\Omega \times [0,T])$. Passing to the limit in the weak formulation of (2.1) guarantees the existence of the limit v, and hence we conclude from the lower semicontinuity of the L^2 norm with respect to weak convergence that the limit (v, α) is a minimizer of (2.2).

To compute the solution of the minimization problem, we will use a quasi-Newton method with limited storage, which is described in section 5.

3. Finite element discretization. We now formulate a finite element method for (2.4) based on using continuous piecewise linear functions in space and time. We discretize $\Omega \times (0,T)$ in the usual way, denoting by $K_h = \{K\}$ a partition of the domain Ω into tetrahedra K ($h = h(x)$ being a mesh function representing the local diameter of the elements), and we let $J_k = \{J = J_1 \cup J_2\}$ be a partition of the time interval $(0,T)$ into time intervals $J = (t_{k-1}, t_k]$ of uniform length $\tau = t_k - t_{k-1}$, where $J_1 = (t_{k-1}, t_k],\ t \in (0, t_1]$, and $J_2 = (t_{k-1}, t_k],\ t \in (t_1, T]$. In fully discrete form, the resulting method corresponds to a centered finite difference approximation for the second-order time derivative and a usual finite element approximation of the Laplacian.

To formulate the finite element method for (2.4) we introduce the finite element spaces V_h, W_h^v, and W_h^λ defined by

$$\begin{aligned}
V_h &:= \{v \in L_2(\Omega) : v \in P_0(K), \forall K \in K_h\}, \\
W_1^v &:= \{v \in H^1(\Omega \times J_1) : v(\cdot, 0) = 0,\ \partial_n v|_{\Gamma_1} = v_1,\ \partial_n v|_{\Gamma_2} = 0\}, \\
W_2^v &:= \{v \in H^1(\Omega \times J_2) : v(\cdot, 0) = 0,\ \partial_n v|_{\Gamma} = 0\}, \\
W^\lambda &:= \{\lambda \in H^1(\Omega \times J) : \lambda(\cdot, T) = 0,\ \partial_n \lambda|_{\Gamma} = 0\}, \\
W_h^v &:= \{v \in W_1^v \cup W_2^v : v|_{K \times (J_1 \cup J_2)} \in P_1(K) \times (P_1(J_1) \cup P_1(J_2)), \forall K \in K_h, \forall J \in J_k\}, \\
W_h^\lambda &:= \{v \in W^\lambda : v|_{K \times J} \in P_1(K) \times P_1(J), \forall K \in K_h, \forall J \in J_k\},
\end{aligned}$$

where $P_1(K)$ and $P_1(J)$ are the sets of linear functions on K and J, respectively.

We define $U_h = W_h^v \times W_h^\lambda \times V_h$. The finite element method now reads: Find $u_h \in U_h$ such that

$$L'(u_h)(\bar{u}) = 0 \quad \forall \bar{u} \in U_h. \tag{3.1}$$

4. Fully discrete scheme. Expanding v, λ in terms of the standard continuous piecewise linear functions $\varphi_i(x)$ in space and $\psi_i(t)$ in time and substituting this into (2.5)–(2.6), we obtain the following system of linear equations:

$$M(\mathbf{v}^{k+1} - 2\mathbf{v}^k + \mathbf{v}^{k-1}) = \tau^2 P_1^k - \tau^2 K \left(\frac{1}{6}\mathbf{v}^{k-1} + \frac{2}{3}\mathbf{v}^k + \frac{1}{6}\mathbf{v}^{k+1} \right), \tag{4.1}$$

$$M(\boldsymbol{\lambda}^{k+1} - 2\boldsymbol{\lambda}^k + \boldsymbol{\lambda}^{k-1}) = -\tau^2 S^k - \tau^2 K \left(\frac{1}{6}\boldsymbol{\lambda}^{k-1} + \frac{2}{3}\boldsymbol{\lambda}^k + \frac{1}{6}\boldsymbol{\lambda}^{k+1} \right), \tag{4.2}$$

with initial conditions for both v and λ:

$$v(0) = \frac{\partial v}{\partial t}(0) = 0, \tag{4.3}$$

$$\lambda(T) = \frac{\partial \lambda}{\partial t}(T) = 0. \tag{4.4}$$

Here, M is the mass matrix in space, K is the stiffness matrix, $k = 1, 2, 3 \ldots$ denotes the time level, F^k, S^k are the load vectors, $\mathbf{v}$ is the unknown discrete field values of v, $\boldsymbol{\lambda}$ is the unknown discrete field values of λ, and τ is the time step.

The explicit formulas for the entries in system (4.1)–(4.2) at each element e can be given as

$$M_{i,j}^e = (\alpha\varphi_i, \varphi_j)_e, \tag{4.5}$$

$$K_{i,j}^e = (\bigtriangledown\varphi_i, \bigtriangledown\varphi_j)_e, \tag{4.6}$$

$$P_{1_{j,m}} = (v_1, \varphi_j\psi_m)_{\Gamma_1 \times J_1}, \tag{4.7}$$

$$S_{j,m}^e = (v - \tilde{v}, \varphi_j\psi_m)_{e \times J}, \tag{4.8}$$

where $(.,.)_e$ denotes the $L_2(e)$ scalar product. The matrix M_e is the contribution from element e to the global assembled matrix in space M, K^e is the contribution from element e to the global assembled matrix K, P_1 is the contribution of the boundary term on Γ_1, and S^e is the contribution from element e to the assembled source vector of the right-hand side of (2.8).

To obtain an explicit scheme we approximate M with the lumped mass matrix M^L, the diagonal approximation obtained by taking the row sum of M; see, e.g., [23]. By multiplying (4.1)–(4.2) with $(M^L)^{-1}$ and replacing the terms $\frac{1}{6}\mathbf{v}^{k-1} + \frac{2}{3}\mathbf{v}^k + \frac{1}{6}\mathbf{v}^{k+1}$ and $\frac{1}{6}\boldsymbol{\lambda}^{k-1} + \frac{2}{3}\boldsymbol{\lambda}^k + \frac{1}{6}\boldsymbol{\lambda}^{k+1}$ by $\mathbf{v}^k$ and $\boldsymbol{\lambda}^k$, respectively, we obtain an efficient explicit formulation:

$$\mathbf{v}^{k+1} = \tau^2 (M^L)^{-1} P_1^k + 2\mathbf{v}^k - \tau^2 (M^L)^{-1} K\mathbf{v}^k - \mathbf{v}^{k-1}, \tag{4.9}$$

$$\boldsymbol{\lambda}^{k-1} = -\tau^2 (M^L)^{-1} S^k + 2\boldsymbol{\lambda}^k - \tau^2 (M^L)^{-1} K\boldsymbol{\lambda}^k - \boldsymbol{\lambda}^{k+1}. \tag{4.10}$$

The discrete version of (2.7) takes the form

$$0 = -\int_0^T \int_\Omega \frac{\partial \lambda_h}{\partial t} \frac{\partial v_h}{\partial t} \bar{\alpha}\, dxdt + \gamma \int_\Omega (\alpha_h - \alpha_0)\bar{\alpha}\, dx, \qquad \forall \bar{\alpha} \in V_h. \tag{4.11}$$

5. Optimization by a quasi-Newton method. To solve the discrete problem (3.1), we use a quasi-Newton method with limited storage [33], where we compute a sequence α_h^k, $k = 0, 1, \dots$, of approximations of α_h with nodal values α_k given by

$$\alpha_{k+1} = \alpha_k - \rho^k H^k g_k. \tag{5.1}$$

Here, the step length ρ^n is computed with a line-search algorithm given in [34], and g_k are the nodal values of the gradient given by

$$g^k(x) = -\int_0^T \frac{\partial \lambda_h^k(x,t)}{\partial t} \frac{\partial v_h^k(x,t)}{\partial t} dt + \gamma(\alpha_k(x) - \alpha_0), \tag{5.2}$$

where v_h^k and λ_h^k solve the discrete analogues of (2.1) and (2.8).

H^k is given by the usual BFGS update formula of the Hessian (cf. [17])

$$H^{k+1} = (I - ds_k y_k^T) H^k (I - dy_k s_k^T) + \rho s_k s_k^T, \tag{5.3}$$

where $d = 1/(y_k^T s_k)$ and

$$s_k = \alpha_{k+1} - \alpha_k, \tag{5.4}$$

$$y_k = g_{k+1} - g_k. \tag{5.5}$$

Note that instead of explicitly computing the Hessian H^k in (5.1), we compute the product $H^{k+1} g^k$ from (5.3) to get

$$((I - ds_k y_k^T) H^k (I - dy_k s_k^T) + \rho s_k s_k^T) g^k = (I - ds_k y_k^T) H^k (g^k - dy_k s_k^T g^k) + \rho s_k s_k^T g^k, \tag{5.6}$$

involving only scalar products of vectors and computing $H^k g^k$ similarly. A modified version of H_k is stored implicitly, by using a certain number m of the vector pairs (s_i, y_i).

6. An a posteriori error estimate for the Lagrangian and an adaptive algorithm.

6.1. A posteriori error estimate. Following [8], we now present the main steps in the proof of an a posteriori error estimate for the Lagrangian. Let C denote various constants of moderate size. We start by writing an equation for the error e in the Lagrangian as

$$\begin{aligned} e = L(u) - L(u_h) &= \int_0^1 \frac{d}{d\epsilon} L(u\epsilon + (1-\epsilon)u_h) d\epsilon \\ &= \int_0^1 L'(u\epsilon + (1-\epsilon)u_h)(u - u_h) d\epsilon = L'(u_h)(u - u_h) + R, \end{aligned} \tag{6.1}$$

where R denotes (a small) second-order term. For full details of the arguments we refer the reader to [3] and [21].

Using the Galerkin orthogonality (3.1), the splitting $u - u_h = (u - u_h^I) + (u_h^I - u_h)$, where u_h^I denotes an interpolant of u, and neglecting the term R, we get the following error representation:

$$e \approx L'(u_h)(u - u_h^I) = (I_1 + I_2 + I_3), \tag{6.2}$$

where

$$I_1 = \int_0^T \int_\Omega \left(-\alpha_h \frac{\partial(\lambda - \lambda_h^I)}{\partial t} \frac{\partial v_h}{\partial t} + \nabla(\lambda - \lambda_h^I) \nabla v_h \right) \, dxdt - \int_0^{t_1} \int_{\Gamma_1} v_1 (\lambda - \lambda_h^I) \, d\Gamma dt, \tag{6.3}$$

$$I_2 = \int_0^T \int_\Omega (v_h - \tilde{v})(v - v_h^I) \, \delta_{obs} \, dxdt + \int_0^T \int_\Omega \left(-\alpha_h \frac{\partial \lambda_h}{\partial t} \frac{\partial (v - v_h^I)}{\partial t} + \nabla \lambda_h \nabla (v - v_h^I) \right) \, dxdt, \tag{6.4}$$

$$I_3 = -\int_0^T \int_\Omega \frac{\partial \lambda_h(x,t)}{\partial t} \frac{\partial v_h(x,t)}{\partial t} (\alpha - \alpha_h^I) \, dxdt + \gamma \int_\Omega (\alpha_h - \alpha_0)(\alpha - \alpha_h^I) dx. \tag{6.5}$$

To estimate (6.3) we integrate by parts in the first and second terms to get

$$\begin{aligned} \left| I_1 \right| = \Bigg| & \int_0^T \int_\Omega \left(\alpha_h \frac{\partial^2 v_h}{\partial t^2} (\lambda - \lambda_h^I) - \triangle v_h (\lambda - \lambda_h^I) \right) \, dxdt \\ & - \int_0^{t_1} \int_{\Gamma_1} v_1 (\lambda - \lambda_h^I) \, d\Gamma dt + \sum_K \int_0^T \int_{\partial K} \frac{\partial v_h}{\partial n_K} (\lambda - \lambda_h^I) \, dsdt \\ & - \sum_k \int_\Omega \alpha_h \left[\frac{\partial v_h}{\partial t}(t_k) \right] (\lambda - \lambda_h^I)(t_k) \, dx \Bigg|, \end{aligned} \tag{6.6}$$

where the terms $\frac{\partial v_h}{\partial n_K}$ and $\left[\frac{\partial v_h}{\partial t}\right]$ appear during the integration by parts and denote the derivative of v_h in the outward normal direction n_K of the boundary ∂K of element K and the jump of the derivative of v_h in time, respectively. In the third term of (6.6) we sum over the element boundaries, and each internal side $S \in S_h$ occurs twice. Denoting by $\partial_s v_h$ the derivative of a function v_h in one of the normal directions of each side S, we can write

$$\sum_K \int_{\partial K} \frac{\partial v_h}{\partial n_K} (\lambda - \lambda_h^I) \, ds = \sum_S \int_S \left[\partial_s v_h \right] (\lambda - \lambda_h^I) \, ds, \tag{6.7}$$

where $\left[\partial_s v_h\right]$ is the jump in the derivative $\partial_s v_h$ computed from the two elements sharing S. We distribute each jump equally to the two sharing triangles and return to a sum over element edges ∂K:

$$\sum_S \int_S \left[\partial_s v_h \right] (\lambda - \lambda_h^I) \, ds = \sum_K \frac{1}{2} h_K^{-1} \int_{\partial K} \left[\partial_s v_h \right] (\lambda - \lambda_h^I) \, h_K \, ds. \tag{6.8}$$

We formally set $dx = h_K ds$ and replace the integrals over the element boundaries ∂K by integrals over the elements K, to get

$$\left| \sum_K \frac{1}{2} h_K^{-1} \int_{\partial K} \left[\partial_s v_h \right] (\lambda - \lambda_h^I) \, h_K \, ds \right| \leq C \max_{S \subset \partial K} h_K^{-1} \int_\Omega \left| \left[\partial_s v_h \right] \right| \cdot \left| (\lambda - \lambda_h^I) \right| \, dx, \tag{6.9}$$

where $\left[\partial_s v_h\right]\big|_K = \max_{S\subset\partial K}\left[\partial_s v_h\right]\big|_S$.

In a similar way we can estimate the fourth term in (6.6):

$$\begin{aligned}\left|\sum_k \int_\Omega \alpha_h\left[\frac{\partial v_h}{\partial t}(t_k)\right](\lambda-\lambda_h^I)(t_k)\ dx\right| &\le \sum_k \int_\Omega \alpha_h\tau^{-1}\cdot\left|\left[\frac{\partial v_h}{\partial t}(t_k)\right]\right|\cdot\left|(\lambda-\lambda_h^I)(t_k)\right|\ \tau dx\\ &\le C\sum_k\int_{J_k}\int_\Omega \alpha_h\tau^{-1}\cdot\left|\left[\partial v_{ht_k}\right]\right|\cdot\left|(\lambda-\lambda_h^I)\right|\,dxdt\\ &= C\int_0^T\int_\Omega \alpha_h\tau^{-1}\cdot\left|\left[\partial v_{ht}\right]\right|\cdot\left|(\lambda-\lambda_h^I)\right|\,dxdt,\end{aligned}\tag{6.10}$$

where

$$[\partial v_{ht_k}] = \max_{J_k}\left(\left[\frac{\partial v_h}{\partial t}(t_k)\right],\ \left[\frac{\partial v_h}{\partial t}(t_{k+1})\right]\right),\tag{6.11}$$

and $[\partial v_{ht}]$ is defined as the maximum of the two jumps in time on each time interval J_k appearing in (6.11):

$$[\partial v_{ht}] = [\partial v_{ht_k}] \quad \text{on } J_k.$$

Substituting both of the above expressions for the second and third terms in (6.6), we get

$$\begin{aligned}\left|I_1\right| \le& \left|\int_0^T\int_\Omega\left(\alpha_h\frac{\partial^2 v_h}{\partial t^2}-\triangle v_h\right)(\lambda-\lambda_h^I)\ dxdt\right|\\ &-\left|\int_0^{t_1}\int_{\Gamma_1} v_1(\lambda-\lambda_h^I)\ d\Gamma dt\right|\\ &+C\int_0^T\int_\Omega \max_{S\subset\partial K} h_k^{-1}\cdot\left|\left[\partial_s v_h\right]\right|\cdot\left|(\lambda-\lambda_h^I)\right|\,dxdt\\ &+C\int_0^T\int_\Omega \alpha_h\tau^{-1}\cdot\left|\left[\partial v_{ht}\right]\right|\cdot\left|(\lambda-\lambda_h^I)\right|\,dxdt.\end{aligned}\tag{6.12}$$

Next, we use a standard interpolation estimate for $\lambda-\lambda_h^I$ to get

$$\begin{aligned}\left|I_1\right| \le& C\int_0^T\int_\Omega\left|\alpha_h\frac{\partial^2 v_h}{\partial t^2}-\triangle v_h\right|\cdot\left(\tau^2\left|\frac{\partial^2\lambda}{\partial t^2}\right|+h^2\left|D_x^2\lambda\right|\right)\ dxdt\\ &-C\int_0^{t_1}\int_{\Gamma_1} v_1\cdot\left(\tau^2\left|\frac{\partial^2\lambda}{\partial t^2}\right|+h^2\left|D_x^2\lambda\right|\right)\ d\Gamma dt\\ &+C\int_0^T\int_\Omega \max_{S\subset\partial K} h_k^{-1}\cdot\left|\left[\partial_s v_h\right]\right|\cdot\left(\tau^2\left|\frac{\partial^2\lambda}{\partial t^2}\right|+h^2\left|D_x^2\lambda\right|\right)\ dxdt\\ &+C\int_0^T\int_\Omega \alpha_h\tau^{-1}\cdot\left|\left[\partial v_{ht}\right]\right|\cdot\left(\tau^2\left|\frac{\partial^2\lambda}{\partial t^2}\right|+h^2\left|D_x^2\lambda\right|\right)\ dxdt.\end{aligned}\tag{6.13}$$

Next, we note that the first integral in (6.13) disappears, since v_h is a continuous piecewise linear function. We then estimate $\frac{\partial^2\lambda}{\partial t^2} \approx \frac{[\partial\lambda_h/\partial t]}{\tau}$ and $D_x^2\lambda \approx \frac{[\partial\lambda_h/\partial n]}{h}$ to get

$$
\begin{aligned}
\left|I_1\right| &\le C\int_0^{t_1}\int_{\Gamma_1}\left|v_1\right|\cdot\left(\tau^2\left|\frac{\left[\frac{\partial\lambda_h}{\partial t}\right]}{\tau}\right|+h^2\left|\frac{\left[\frac{\partial\lambda_h}{\partial n}\right]}{h}\right|\right)\,d\Gamma dt\\
&+ C\int_0^T\int_\Omega \max_{S\subset\partial K} h_k^{-1}\left|\left[\partial_s v_h\right]\right|\cdot\left(\tau^2\left|\frac{\left[\frac{\partial\lambda_h}{\partial t}\right]}{\tau}\right|+h^2\left|\frac{\left[\frac{\partial\lambda_h}{\partial n}\right]}{h}\right|\right)\,dxdt\\
&+ C\int_0^T\int_\Omega \alpha_h\tau^{-1}\left|\left[\partial v_{ht}\right]\right|\cdot\left(\tau^2\left|\frac{\left[\frac{\partial\lambda_h}{\partial t}\right]}{\tau}\right|+h^2\left|\frac{\left[\frac{\partial\lambda_h}{\partial n}\right]}{h}\right|\right)\,dxdt.
\end{aligned}
\tag{6.14}
$$

We estimate I_2 similarly:

$$
\begin{aligned}
\left|I_2\right| &\le \int_0^T\int_\Omega\left|\left(\alpha_h\frac{\partial^2\lambda_h}{\partial t^2}(v-v_h^I)-\triangle\lambda_h(v-v_h^I)-(v_h-\tilde v)(v-v_h^I)\right)\right|\,dxdt\\
&+ C\int_0^T\int_\Omega \max_{S\subset\partial K} h_k^{-1}\cdot\left|\left[\partial_s\lambda_h\right]\right|\cdot\left|(v-v_h^I)\right|\,dxdt\\
&+ C\int_0^T\int_\Omega \alpha_h\tau^{-1}\cdot\left|\left[\partial\lambda_{ht}\right]\right|\cdot\left|(v-v_h^I)\right|\,dxdt\\
&\le C\int_0^T\int_\Omega\left|\left(\alpha_h\frac{\partial^2\lambda_h}{\partial t^2}-\triangle\lambda_h-(v_h-\tilde v)\right)\right|\cdot\left|(v-v_h^I)\right|\,dxdt\\
&+ C\int_0^T\int_\Omega \max_{S\subset\partial K} h_k^{-1}\cdot\left|\left[\partial_s\lambda_h\right]\right|\cdot\left|(v-v_h^I)\right|\,dxdt\\
&+ C\int_0^T\int_\Omega \alpha_h\tau^{-1}\cdot\left|\left[\partial\lambda_{ht}\right]\right|\cdot\left|(v-v_h^I)\right|\,dxdt\\
&\le C\int_0^T\int_\Omega\left|\left(\alpha_h\frac{\partial^2\lambda_h}{\partial t^2}-\triangle\lambda_h-(v_h-\tilde v)\right)\right|\left(\tau^2\left|\frac{\partial^2 v}{\partial t^2}\right|+h^2\left|D_x^2 v\right|\right)\,dxdt\\
&+ C\int_0^T\int_\Omega \max_{S\subset\partial K} h_k^{-1}\cdot\left|\left[\partial_s\lambda_h\right]\right|\left(\tau^2\left|\frac{\partial^2 v}{\partial t^2}\right|+h^2\left|D_x^2 v\right|\right)\,dxdt\\
&+ C\int_0^T\int_\Omega \alpha_h\tau^{-1}\cdot\left|\left[\partial\lambda_{ht}\right]\right|\cdot\left(\tau^2\left|\frac{\partial^2 v}{\partial t^2}\right|+h^2\left|D_x^2 v\right|\right)\,dxdt\\
&\le C\int_0^T\int_\Omega\left|(v_h-\tilde v)\right|\cdot\left(\tau^2\left|\frac{\left[\frac{\partial v_h}{\partial t}\right]}{\tau}\right|+h^2\left|\frac{\left[\frac{\partial v_h}{\partial n}\right]}{h}\right|\right)\,dxdt\\
&+ C\int_0^T\int_\Omega \max_{S\subset\partial K} h_k^{-1}\left|\left[\partial_s\lambda_h\right]\right|\cdot\left(\tau^2\left|\frac{\left[\frac{\partial v_h}{\partial t}\right]}{\tau}\right|+h^2\left|\frac{\left[\frac{\partial v_h}{\partial n}\right]}{h}\right|\right)\,dxdt\\
&+ C\int_0^T\int_\Omega \alpha_h\tau^{-1}\cdot\left|\left[\partial\lambda_{ht}\right]\right|\cdot\left(\tau^2\left|\frac{\left[\frac{\partial v_h}{\partial t}\right]}{\tau}\right|+h^2\left|\frac{\left[\frac{\partial v_h}{\partial n}\right]}{h}\right|\right)\,dxdt.
\end{aligned}
\tag{6.15}
$$

To estimate I_3 we use a standard approximation estimate of the form $\alpha - \alpha_h^I \approx hD_x\alpha$ to get

$$
\begin{aligned}
\big|I_3\big| &\le \int_0^T \int_\Omega \left| \frac{\partial \lambda_h(x,t)}{\partial t} \cdot \frac{\partial v_h(x,t)}{\partial t} \right| \cdot h \cdot \big|D_x\alpha\big| \, dxdt \\
&\quad + \gamma \int_\Omega (\alpha_h - \alpha_0) h \cdot \big|D_x\alpha\big| \, dx \\
&\le C \int_0^T \int_\Omega \left| \frac{\partial \lambda_h(x,t)}{\partial t} \cdot \frac{\partial v_h(x,t)}{\partial t} \right| \cdot h \cdot \left| \frac{[\alpha_h]}{h} \right| \, dxdt \\
&\quad + C\gamma \int_\Omega |\alpha_h - \alpha_0| \cdot h \cdot \left| \frac{[\alpha_h]}{h} \right| \, dx \\
&\le C \int_0^T \int_\Omega \left| \frac{\partial \lambda_h(x,t)}{\partial t} \cdot \frac{\partial v_h(x,t)}{\partial t} \right| \cdot \big|[\alpha_h]\big| \, dxdt \\
&\quad + C\gamma \int_\Omega |\alpha_h - \alpha_0| \cdot \big|[\alpha_h]\big| \, dx.
\end{aligned}
\tag{6.16}
$$

We therefore obtain the following result.

THEOREM 6.1. *Let $L(u) = L(v, \lambda, \alpha)$ be the Lagrangian defined in* (2.3)*, and let $L(u_h) = L(v_h, \lambda_h, \alpha_h)$ be the approximation of $L(u)$. Then the following error representation formula for the error e in the Lagrangian holds:*

$$
\begin{aligned}
\big|e\big| \le \Bigg(&\int_0^{t_1} \int_{\Gamma_1} R_{v_1}\sigma_\lambda \, d\Gamma dt + \int_0^T \int_\Omega R_{v_2}\sigma_\lambda \, dxdt + \int_0^T \int_\Omega R_{v_3}\sigma_\lambda \, dxdt \\
&+ \int_0^T \int_\Omega R_{\lambda_1}\sigma_v \, dxdt + \int_0^T \int_\Omega R_{\lambda_2}\sigma_v \, dxdt + \int_0^T \int_\Omega R_{\lambda_3}\sigma_v \, dxdt \\
&+ \int_0^T \int_\Omega R_{\alpha_1}\sigma_\alpha \, dxdt + \int_\Omega R_{\alpha_2}\sigma_\alpha \, dx \Bigg),
\end{aligned}
\tag{6.17}
$$

where the residuals are defined by

$$
R_{v_1} = \big|v_1\big|, \quad R_{v_2} = \max_{S \subset \partial K} h_k^{-1} \big|\big[\partial_s v_h\big]\big|, \quad R_{v_3} = \alpha_h \tau^{-1} \big|\big[\partial v_{ht}\big]\big|, \tag{6.18}
$$

$$
R_{\lambda_1} = \big|v_h - \tilde{v}\big|, \quad R_{\lambda_2} = \max_{S \subset \partial K} h_k^{-1} \big|\big[\partial_s \lambda_h\big]\big|, \quad R_{\lambda_3} = \alpha_h \tau^{-1} \big|\big[\partial \lambda_{ht}\big]\big|, \tag{6.19}
$$

$$
R_{\alpha_1} = \left| \frac{\partial \lambda_h}{\partial t} \right| \cdot \left| \frac{\partial v_h}{\partial t} \right|, \quad R_{\alpha_2} = \gamma |\alpha_h - \alpha_0|, \tag{6.20}
$$

and the interpolation errors are

$$
\sigma_\lambda = C\tau \left| \left[\frac{\partial \lambda_h}{\partial t} \right] \right| + Ch \left| \left[\frac{\partial \lambda_h}{\partial n} \right] \right|, \tag{6.21}
$$

$$
\sigma_v = C\tau \left| \left[\frac{\partial v_h}{\partial t} \right] \right| + Ch \left| \left[\frac{\partial v_h}{\partial n} \right] \right|, \tag{6.22}
$$

$$
\sigma_\alpha = C\big|[\alpha_h]\big|. \tag{6.23}
$$

Note that R_{α_2} corresponds to the penalty term added in the Tikhonov regularization of (2.2). Indeed, as γ tends to zero, the error term R_{α_1} will dominate, and in the limit we arrive at the error estimator for the Lagrangian without regularization.

6.2. Adaptive algorithm. The main goal in adaptive error control for the Lagrangian is to find a mesh K_h with as few nodes as possible, such that $\|L(u) - L(u_h)\| < tol$. Instead of finding $L(u)$ analytically, we will use the a posteriori error estimate: We shall find a partition K_h such that the corresponding finite element approximation $L(u_h)$ satisfies

$$\begin{aligned}\Bigg(&\int_0^{t_1}\int_{\Gamma_1} R_{v_1}\sigma_\lambda \, d\Gamma dt + \int_0^T\int_\Omega R_{v_2}\sigma_\lambda \, dxdt + \int_0^T\int_\Omega R_{v_3}\sigma_\lambda \, dxdt \\ &+ \int_0^T\int_\Omega R_{\lambda_1}\sigma_v \, dxdt + \int_0^T\int_\Omega R_{\lambda_2}\sigma_v \, dxdt + \int_0^T\int_\Omega R_{\lambda_3}\sigma_v \, dxdt \\ &+ \int_0^T\int_\Omega R_{\alpha_1}\sigma_\alpha \, dxdt + \int_\Omega R_{\alpha_2}\sigma_\alpha \, dx\Bigg) < tol.\end{aligned} \tag{6.24}$$

The solution is found by an iterative process, where we start with a coarse mesh and successively refine the mesh by using the stopping criterion (6.24) with a view of using the minimal possible number of elements. More precisely, in the computations below we shall use the following adaptive algorithm:

1. Choose an initial mesh K_h and an initial time partition J_k of the time interval $(0, T)$.
2. Compute the solution v of the forward problem (2.1) on K_h and J_k with $\alpha = \alpha^{(n)}$.
3. Compute the solution λ of the adjoint problem (2.8) on K_h and J_k.
4. Update the velocity on K_h and J_k according to

$$\alpha^{(n+1)}(x) = \alpha^{(n)}(x) + \rho^{(n)}\left(\int_0^T \frac{\partial\lambda^n(x,t)}{\partial t}\frac{\partial v^n(x,t)}{\partial t}dt + \gamma(\alpha^{(n)}(x) - \alpha_0)\right).$$

   Repeat steps 1–4 as long as the gradient quickly decreases.
5. Refine all elements where $(R_{\alpha_1} + R_{\alpha_2})\sigma_\alpha > tol$, and construct a new mesh K_h and a new time partition J_k. Here tol is a tolerance chosen by the user. Return to 1.

7. Numerical examples. We illustrate the efficiency and the performance of the hybrid FEM/FDM method on an inverse scattering problem for scanning acoustic microscopy in three dimensions. The geometry of the problem (see Figure 1.1) is taken from a specific microscope (WinSAM 2000, KSI Germany). The computational domain is set as $\Omega = [-10.0, 10.0] \times [-14.0, 16.0] \times [-10.0, 10.0]$, which is split into a finite element domain $\Omega_{FEM} = [-9.0, 9.0] \times [-10.0, -12.0] \times [-9.0, 9.0]$, with an unstructured mesh, and a surrounding domain Ω_{FDM}, with a structured mesh. The space mesh in Ω_{FEM} consists of tetrahedra and in Ω_{FDM} of hexahedra with mesh size $h = 1.0$. We apply the hybrid finite element/difference method presented in [10] with finite elements in Ω_{FEM} and finite differences in Ω_{FDM}. At all boundaries of Ω we use first-order absorbing boundary conditions [19].

The forced acoustic field consists of a wave $v = (v_1, v_2, v_3)$ given as

$$v_i(x, y, z, t)|_{y=0} = -\left(\frac{\sin(100t - \pi/2) + 1}{10}\right) \cdot n_i, \qquad 0 \le t \le \frac{2\pi}{100}, \tag{7.1}$$

which initiates at the spherical boundary Γ_1 of the lens in Ω_{FEM} and propagates in normal direction $n = (n_1, n_2, n_3)$ into Ω. This acoustic field is a simple model of the

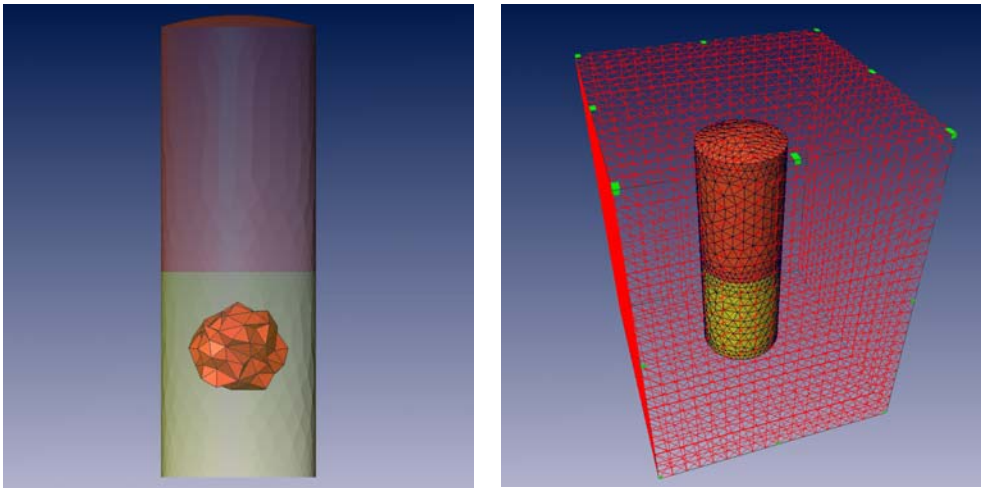

(A) *Geometry of the microscope with inclusion to be reconstructed.*

(B) *Surrounding mesh (outlined) with overlapping nodes at the boundary.*

FIG. 7.1. *Original mesh for computational domain* Ω_{FEM}.

high-frequency excitation pulse generated by the transducer of the microscope. For real data, of course, it is advisable to take the source wavelet used in the specific microscope (which is known). As mentioned in the introduction, due to the multilevel strategy of our adaptive algorithm, we expect convergence for such multimodal sources as well. The observation points are also placed on Γ_1, corresponding to our application, where the same transducer records the reflected waves.

In all the computational tests we chose a time step τ according to the Courant–Friedrichs–Levy (CFL) stability condition

$$\tau \leq \frac{h}{ac_{\max}}, \tag{7.2}$$

where h is the minimal local mesh size, $c_{\max}$ is an a priori upper bound for the coefficient c, and a is a constant.

To improve the reconstruction and achieve better convergence we use the adaptive algorithm described in section 6.2. As we see from Theorem 6.1, the error in the Lagrangian consists of space-time integrals of different residuals multiplied by the interpolation errors. Thus, to estimate the error in the Lagrangian, we need to compute approximated values of $(v_h, \lambda_h, \alpha_h)$ together with residuals and interpolation errors. Since the residuals $R_{\alpha_1}, R_{\alpha_2}$ dominate, we neglect the terms $R_{v_2}, R_{v_3}, R_{\lambda_2}, R_{\lambda_3}$ in computation of the a posteriori error estimator. Further, we also neglect computation of the residuals R_{v_1}, R_{λ_1} since they indicate the error in the upper cylinder of the acoustic microscope, where we already know the value of $c(x) = c_0$. In the current work, the local refinement is based on the residuals since they already give good indications of where to adapt the mesh. The interpolation errors can be obtained following [9] by computing the Hessian of the Lagrangian, and will be included as part of a future work. Thus, the solution of the optimization problem is found in an iterative process, where we start with a coarse mesh shown in Figure 7.1 and evaluate the residuals by computing the Jacobian of the Lagrangian when the L^2 norm of $v - v_{obs}$ stops decreasing in the quasi-Newton iteration. Then we refine this mesh locally where the residuals are largest and construct a new time partition using

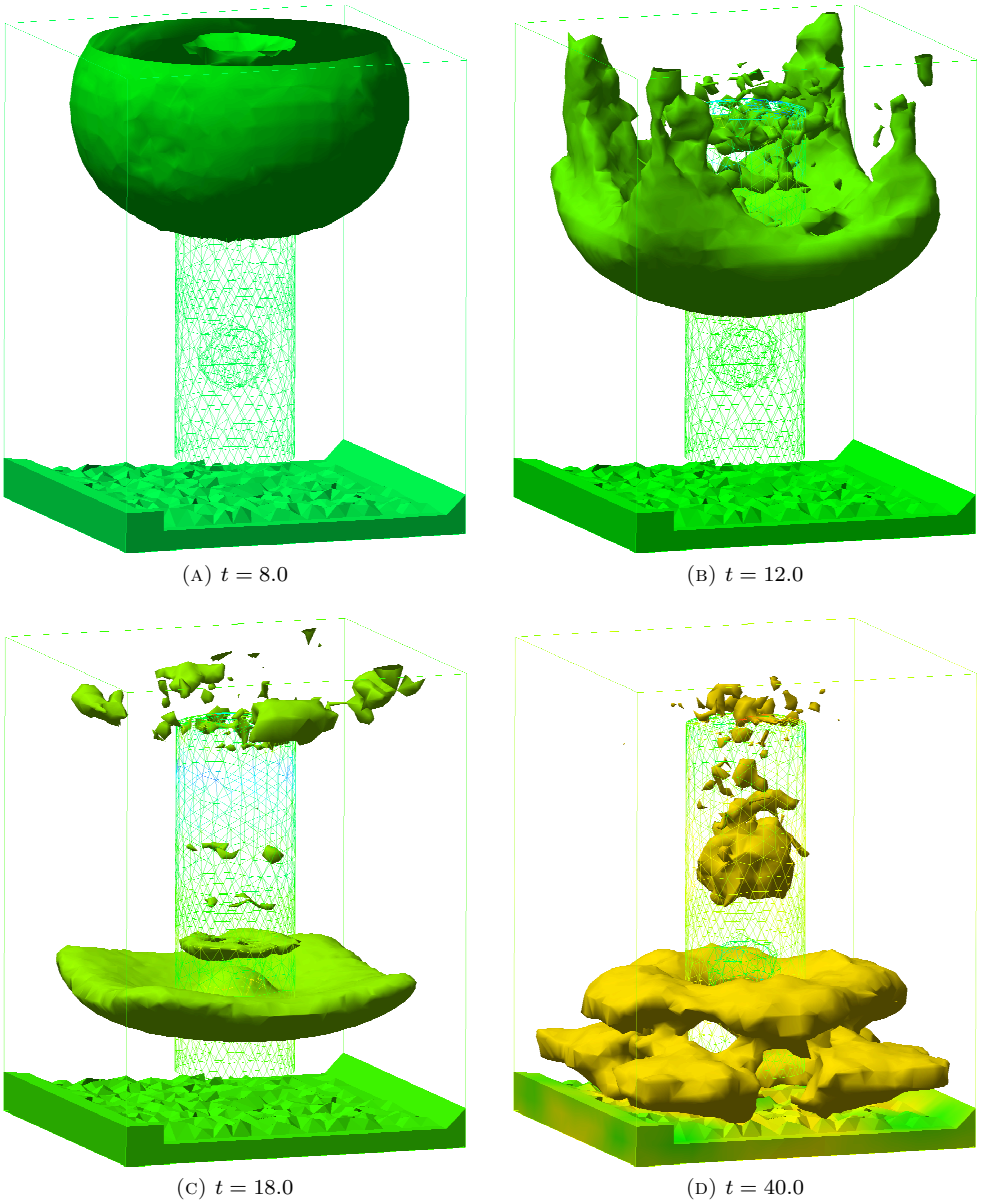

(A) $t = 8.0$ (B) $t = 12.0$

(C) $t = 18.0$ (D) $t = 40.0$

FIG. 7.2. *Solution of the forward problem* (4.9) *with exact value of the parameter* $c = 0.5$ *inside a spherical inclusion and* $c = 1.0$ *everywhere else in* Ω. *We show isosurfaces of the computed solution at different times inside* Ω_{FEM}.

(7.2). In all optimization steps, the number of stored corrections in the quasi-Newton method is $m = 5.0$.

To generate the data at the observation points, we solve the forward problem in the time interval $t = [0, 40.0]$ with the exact value of the parameter $c = 0.5$ inside a spherical inclusion and $c = 1.0$ everywhere else in Ω. In Figure 7.2 we present isosurfaces of the acoustic wavefield (i.e., the solution of the forward problem (4.9) with exact parameters) at different times inside Ω_{FEM}. The deformation of the wave

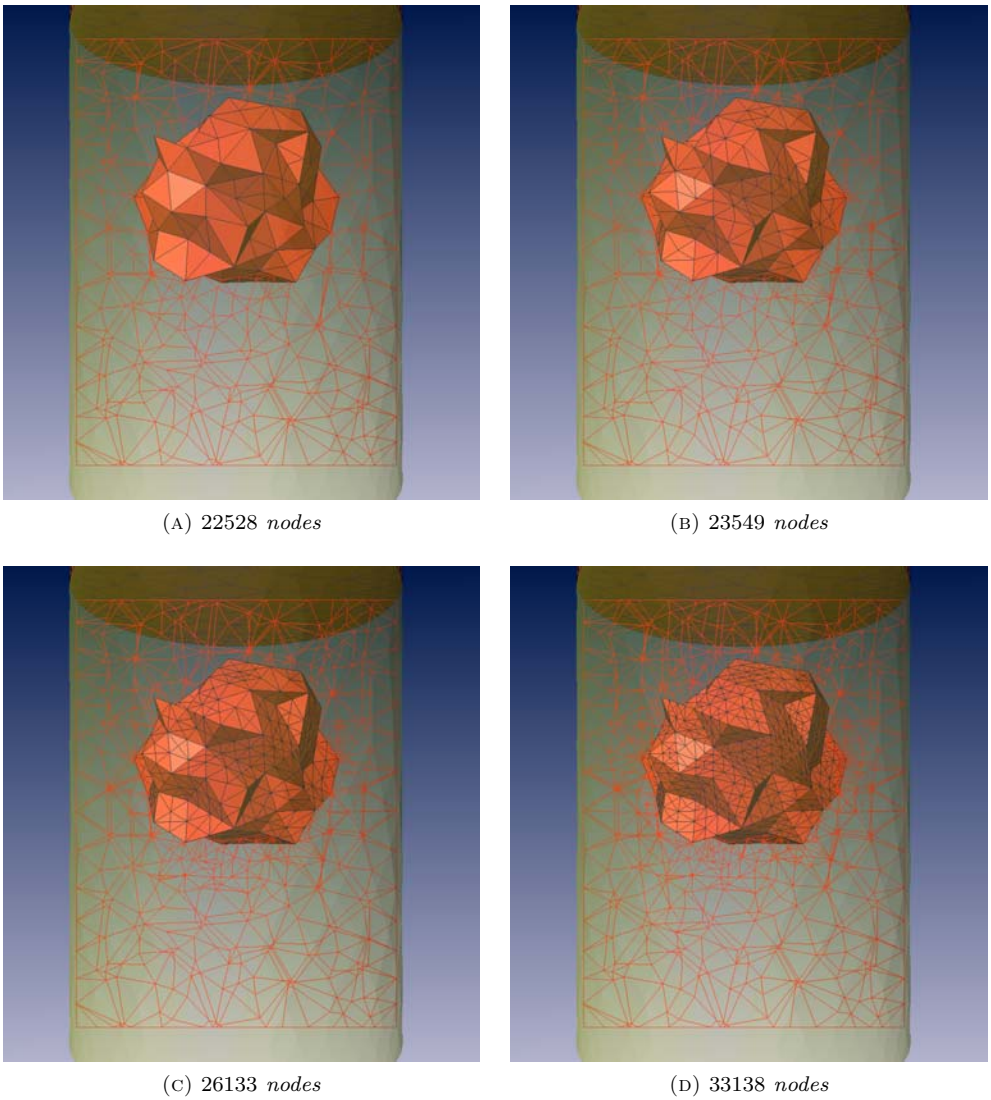

(A) 22528 *nodes* (B) 23549 *nodes*

(C) 26133 *nodes* (D) 33138 *nodes*

FIG. 7.3. *Successive adaptive refinements of the original mesh.*

packet due to the presence of the inclusion leads to reflections traveling back to the observation points, carrying information about the obstacle.

We start the optimization algorithm with guess values of the parameter $c = 1.0$ at all points in the computational domain and a regularization parameter $\gamma = 0.1$. The computations were performed on the four adaptively refined meshes shown in Figure 7.3. Here, we solved the adjoint problem backward in time from $t = 40.0$ down to $t = 0.0$. In Figure 7.4 we display isosurfaces of the computed solution of the adjoint problem on different adaptively refined meshes at the time $t = 0.0$. We observe that the isosurfaces of the adjoint solution are concentrated around the interface between the two cylinders and in the inclusion. There we will also perform local refinement of the mesh, since the residual R_{α_1} in the a posteriori error estimator includes the term $\left|\frac{\partial \lambda_h}{\partial t}\right|$ involving solution of the adjoint problem. In Figure 7.5 we show a comparison

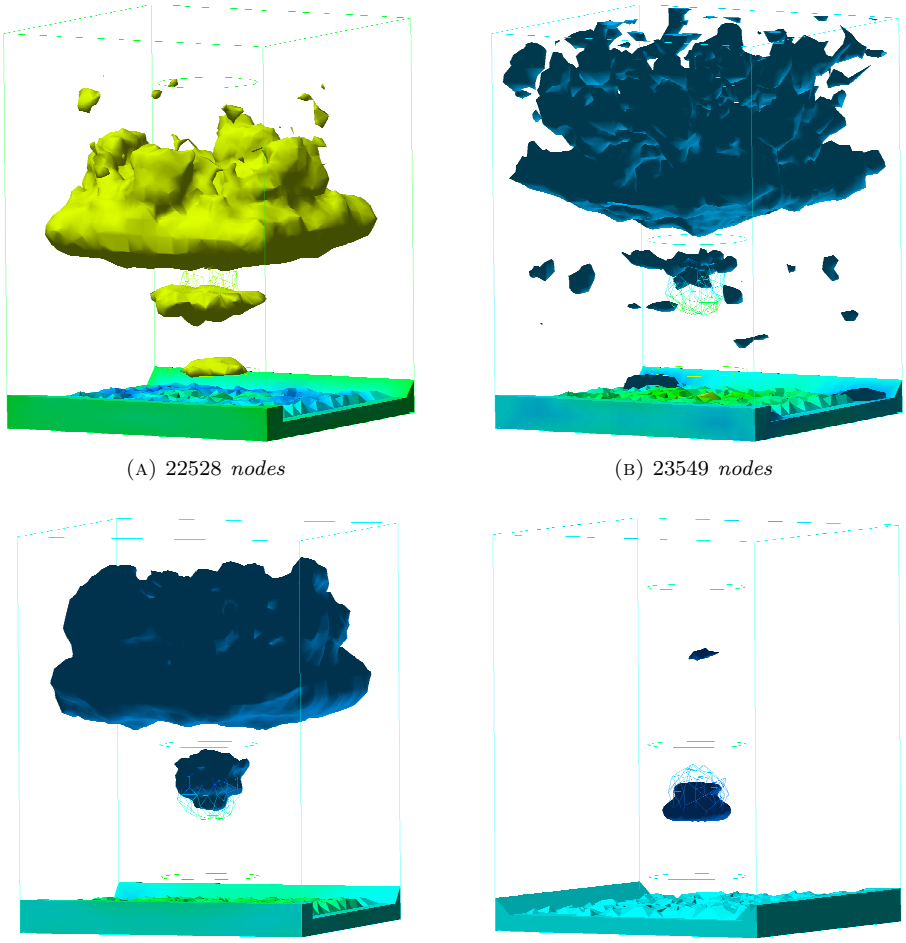

(A) 22528 *nodes* (B) 23549 *nodes*

(C) 26133 *nodes* (D) 33138 *nodes*

FIG. 7.4. *Isosurfaces of the adjoint problem solution on different adaptively refined meshes. We show the solution on the third optimization iteration at time* $t = 0.0$ *in* Ω_{FEM}.

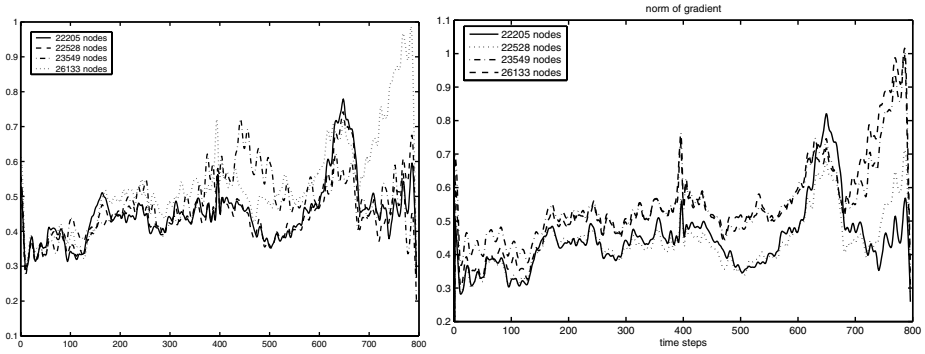

(A) R_{α_1} (B) $||\frac{\partial L}{\partial \alpha}||$

FIG. 7.5. *Comparison of* (A) R_{α_1} *and* (B) $||\frac{\partial L}{\partial \alpha}||$ *on different adaptively refined meshes. We present the smallest value of* R_{α_1} *and* $||\frac{\partial L}{\partial \alpha}||$ *on the corresponding meshes. Here the* x*-axis denotes time steps on* $[0, 40]$.

of R_{α_1} and $||\frac{\partial L}{\partial \alpha}||$ over the time interval $[0, 40]$ on different adaptively refined meshes. Here, the smallest values of the residual R_{α_1} and the L^2 norm in space of $\frac{\partial L}{\partial \alpha}$ are shown on the corresponding meshes.

The L^2 norms in space of the adjoint solution λ_h over the time interval $[0, 40]$ on different optimization iterations on adaptively refined meshes are shown in Figure 7.6. Figure 7.6(A)–(E) display the norm at each optimization iteration on the different

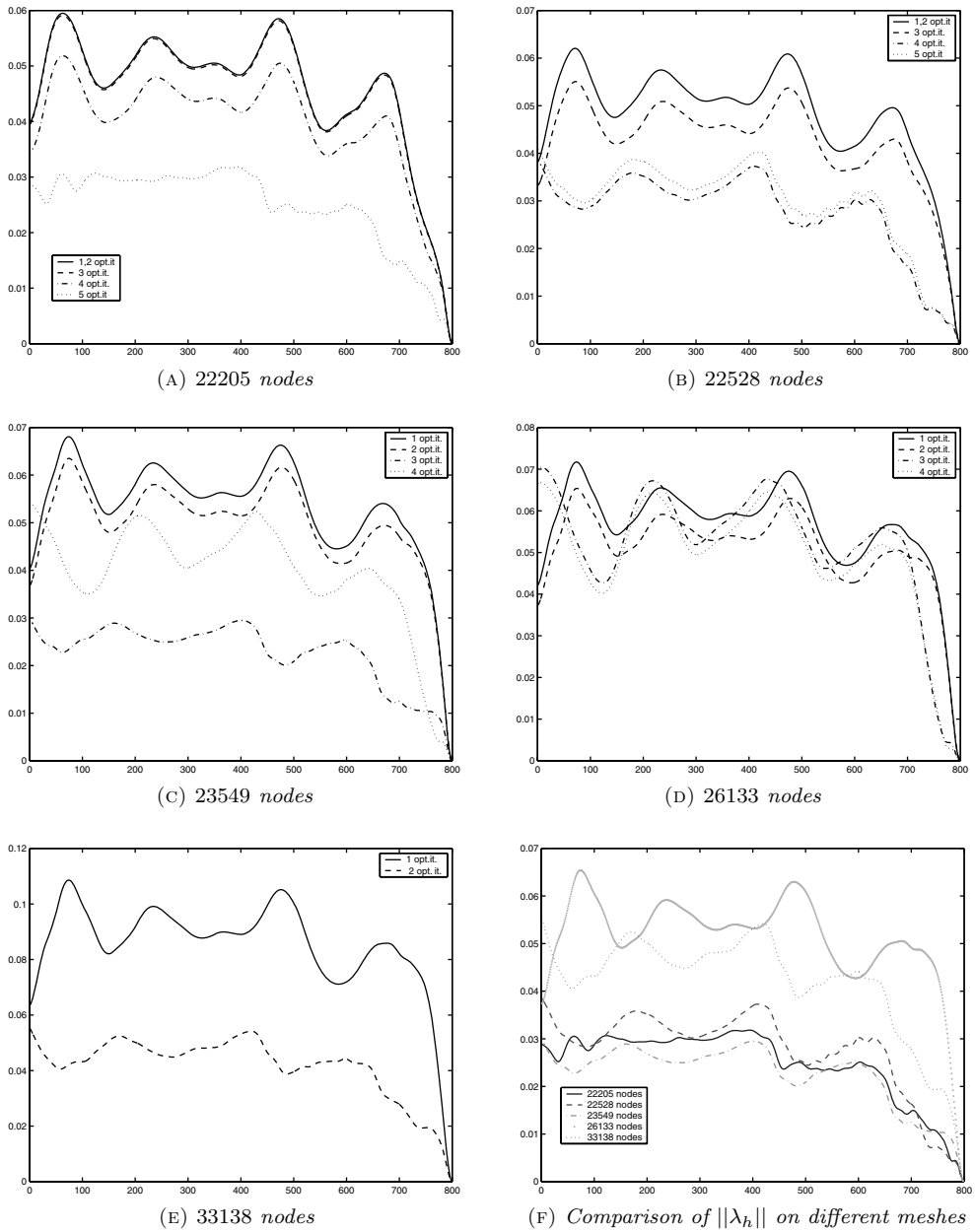

(A) 22205 *nodes* (B) 22528 *nodes*

(C) 23549 *nodes* (D) 26133 *nodes*

(E) 33138 *nodes* (F) *Comparison of* $||\lambda_h||$ *on different meshes*

FIG. 7.6. (A)–(E) L^2 *norms in space of the adjoint problem solution* λ_h *on adaptively refined meshes at different optimization iterations,* (F) *comparison of* $||\lambda_h||$ *on different adaptively refined meshes. Here the x-axis denotes time steps on* $[0, 40]$.

TABLE 7.1. $||v - v_{obs}||$ *on adaptively refined meshes.*

Opt.it.	22205 nodes	22528 nodes	23549 nodes	26133 nodes	33138 nodes
1	0.0506618	0.059448	0.0698214	0.0761904	0.120892
2	0.050106	0.0594441	0.0612598	0.063955	0.0358431
3	0.0358798	0.0465678	0.028501	0.0618176	
4	0.0244553	0.0413165			
5	0.0219676				

adaptively refined meshes. The norm of the adjoint solution decreases faster on finer meshes. Figure 7.6(F) shows a comparison of the L^2 norms in space of the adjoint solution λ_h on different meshes. Here, we present the smallest L^2 norm of λ_h on the corresponding meshes.

In Table 7.1 we give computed L^2 norms of $v - v_{obs}$ on different adaptively refined meshes at each optimization iteration while the norms decrease. The computational tests show that the best results are obtained on a four times adaptively refined mesh, where $||v - v_{obs}||$ is reduced approximately by a factor four between two optimization iterations. We note that the L^2 norms in space and time of $v - v_{obs}$ differ from coarser to finer meshes because of the increase in the number of observation points at the lens boundary during the refinement procedure. This also means that we capture higher and higher frequency content of the data with each refinement step.

The reconstructed parameter c on different adaptively refined meshes in the final optimization iteration is presented in Figure 7.7. We show isosurfaces of the parameter field $c(x)$, indicating domains with a given parameter value. We see that although the qualitative reconstruction on the coarse grid is already good enough to recover the shape of the inclusion even from limited boundary data, the quantitative reconstruction becomes acceptable only on the refined grids. Additionally, with successive refinement, the boundary of the reconstructed inclusion becomes sharper (compare the isosurface in Figure 7.7(A), (B) with those in Figure 7.7(D), (E)). On the grid with 33138 nodes (Figure 7.7(F)), the parameter in the inclusion is calculated as $c \approx 0.51$, compared to the exact value of $c = 0.5$.

However, since the quasi-Newton method is only locally convergent, the values of the identified parameters are very sensitive to the starting values of the parameters in the optimization algorithm and also to the values of the regularization parameter γ and step length ρ in the velocity upgrade. Therefore, to achieve more stable reconstruction, we enforce that the parameter c belongs to C_M by putting box constraints on the computed parameters and using a smoothness indicator to update values of c at the new optimization iteration by local averaging over the neighboring elements.

8. Conclusion. We present an explicit, adaptive, hybrid FEM/FDM method for an inverse scattering problem in scanning acoustic microscopy. The method is hybrid in the sense that different numerical methods, finite elements and finite differences, are used in different parts of the computational domain. The adaptivity is based on a posteriori error estimates for the associated Lagrangian in the form of space-time integrals of residuals multiplied by dual weights, which allows stable reconstruction of a parameter from data given on only a small part of the boundary. Their usefulness for adaptive error control is illustrated on an inverse scattering problem for scanning acoustic microscopy in three dimensions. Future work is concerned with choosing optimal regularization parameters for the functional to be minimized, and extending the adaptive algorithm to use an a posteriori error estimator for the parameter by solving an associated problem for the Hessian of the Lagrangian.

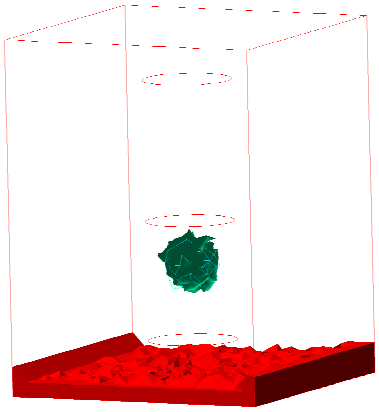

(A) 22528 *nodes,* $c \approx 0.66$

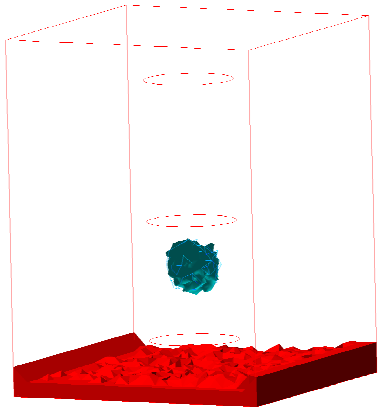

(B) 22528 *nodes,* $c \approx 0.623$

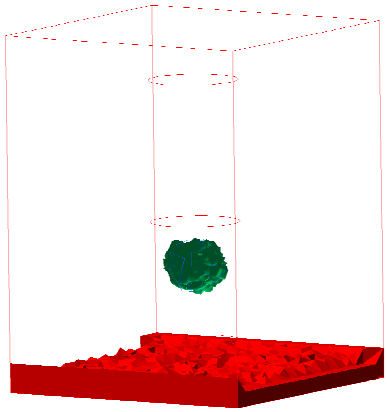

(C) 23549 *nodes,* $c \approx 0.556$

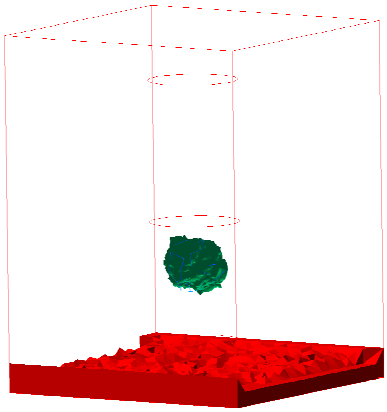

(D) 26133 *nodes,* $c \approx 0.547$

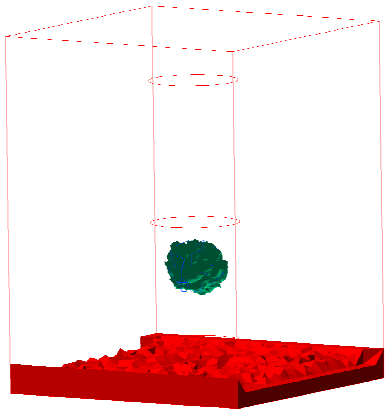

(E) 26133 *nodes,* $c \approx 0.531$

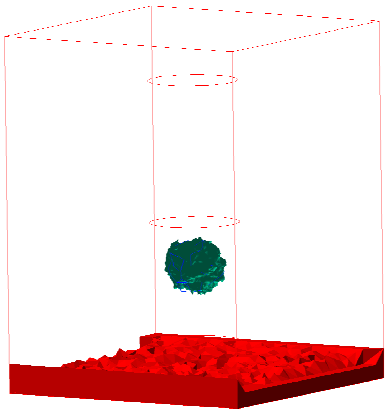

(F) 33138 *nodes,* $c \approx 0.51$

FIG. 7.7. *Reconstructed parameter* $c(x)$ *on different adaptively refined meshes. Isosurfaces of the parameter field* $c(x)$*, indicating domains with a given parameter value, are shown.*

Acknowledgments. We thank Prof. Mikhail Klibanov and Dr. Maxim Shishlenin for useful comments and suggestions. We would also like to express our thanks to both referees for their comments and suggestions on improving the presentation.

REFERENCES

[1] V. Akcelik, G. Biros, and O. Ghattas, *Parallel multiscale Gauss–Newton–Krylov methods for inverse wave propagation*, in Supercomputing '02: Proceedings of the 2002 ACM/IEEE conference on Supercomputing, Los Alamitos, CA, 2002, IEEE Computer Society Press, Piscataway, NJ, pp. 1–15.

[2] C. Bardos, G. Lebeau, and J. Rauch, *Sharp sufficient conditions for the observation, control, and stabilization of waves from the boundary*, SIAM J. Control Optim., 30 (1992), pp. 1024–1065.

[3] R. Becker and R. Rannacher, *An optimal control approach to a posteriori error estimation in finite element methods*, in Acta Numerica, 2001, Acta Numer., Cambridge University Press, Cambridge, UK, 2001, pp. 1–102.

[4] L. Beilina, *Adaptive FEM method for an inverse scattering problem*, J. Inverse Problems Inform. Tech., 3 (2002), pp. 73–116.

[5] L. Beilina, *Adaptive hybrid finite element/difference methods: Application to inverse elastic scattering*, J. Inverse Ill-posed Problems, 6 (2003), pp. 585–618.

[6] L. Beilina, *A hybrid FEM/FDM method for elastic waves*, J. Appl. Comput. Math., 2 (2003), pp. 13–29.

[7] L. Beilina, *Adaptive finite element/difference method for inverse elastic scattering waves*, J. Appl. Comput. Math., 2 (2004), pp. 158–174.

[8] L. Beilina and C. Johnson, *A hybrid FEM/FDM method for an inverse scattering problem*, in Numerical Mathematics and Advanced Applications—ENUMATH 2001, Springer-Verlag, Berlin, 2001, pp. 545–556.

[9] L. Beilina and C. Johnson, *A posteriori error estimation in computational inverse scattering*, Math. Models Methods Appl. Sci., 15 (2005), pp. 23–37.

[10] L. Beilina, K. Samuelsson, and K. Ahlander, *Efficiency of a hybrid method for the wave equation*, in Finite Element Methods (Jyväskylä 2000), GAKUTO Internat. Ser. Math. Sci. Appl. 15, Gakkotosho, Tokyo, 2001, pp. 9–21.

[11] M. I. Belishev and Y. V. Kurylev, *Boundary control, wave field continuation and inverse problems for the wave equation*, Appl. Comp. Math., 22 (1991), pp. 27–52.

[12] A. Briggs, *Acoustic Microscopy*, Clarendon Press, Oxford, UK, 1992.

[13] A. Bukhgeim and M. Klibanov, *Global uniqueness of a class of multidimensional inverse problems*, Sov. Math. Dokl., 24 (1981), pp. 244–247.

[14] C. Bunks, F. M. Saleck, S. Zaleski, and G. Chavent, *Multiscale seismic waveform inversion*, Geophysics, 60 (1995), pp. 1457–1473.

[15] G. Chavent and C. A. Jacewitz, *Determination of background velocities by multiple migration fitting*, Geophys., 60 (1995), pp. 476–490.

[16] D. Colton, J. Coyle, and P. Monk, *Recent developments in inverse acoustic scattering theory*, SIAM Rev., 42 (2000), pp. 369–414.

[17] J. E. Dennis, Jr., and J. J. Moré, *Quasi-Newton methods, Motivation and theory*, SIAM Rev., 19 (1977), pp. 46–89.

[18] H. W. Engl, M. Hanke, and A. Neubauer, *Regularization of Inverse Problems*, Kluwer Academic Publishers, Dordrecht, The Netherlands, 1996.

[19] B. Engquist and A. Majda, *Absorbing boundary conditions for the numerical simulation of waves*, Math. Comp., 31 (1977), pp. 629–651.

[20] K. Eriksson, D. Estep, P. Hansbo, and C. Johnson, *Introduction to adaptive methods for differential equations*, in Acta Numerica, 1995, Acta Numer., Cambridge University Press, Cambridge, UK, 1995, pp. 105–158.

[21] K. Eriksson, D. Estep, P. Hansbo, and C. Johnson, *Computational Differential Equations*, Studentlitteratur/Cambridge University Press, Lund, Sweden/Cambridge, UK, 1996.

[22] X. Feng, S. Lenhart, V. Protopopescu, L. Rachele, and B. Sutton, *Identification problem for the wave equation with Neumann data input and Dirichlet data observations*, Nonlinear Anal., 52 (2003), pp. 1777–1795.

[23] T. J. R. Hughes, *The Finite Element Method*, Prentice–Hall, Englewood Cliffs, NJ, 1987.

[24] M. Ikawa, *Hyperbolic Partial Differential Equations and Wave Phenomena*, American Mathematical Society, Providence, RI, 2000.

[25] O. Y. Imanuvilov and M. Yamamoto, *Global uniqueness and stability in determining coefficients of wave equations*, Comm. Partial Differential Equations, 26 (2001), pp. 1409–1425.
[26] V. Isakov, *Inverse Problems for Partial Differential Equations*, Springer, Berlin, 1998.
[27] C. Johnson, *Adaptive computational methods for differential equations*, in ICIAM99, Oxford University Press, Oxford, UK, 2000, pp. 96–104.
[28] J. Kaipio and E. Somersalo, *Statistical and Computational Inverse Problems*, Springer, Berlin, 2005.
[29] M. Klibanov and A. A. Timonov, *Carleman estimates for coefficient inverse problems and numerical applications*, VSP Publishing, Utrecht, The Netherlands, 2004.
[30] J. L. Lions, *Optimal Control of Systems Governed by Partial Differential Equations*, Springer, Berlin, 1971.
[31] J. L. Lions and E. Magenes, *Non-Homogeneous Boundary Value Problems and Applications. Vols.* I *and* II, Springer-Verlag, Berlin, 1972.
[32] F. Natterer and F. Wubbeling, *A propagation-backpropagation method for ultrasound tomography*, Inverse Problems, 11 (1995), pp. 1225–1232.
[33] J. Nocedal, *Updating quasi-Newton matrices with limited storage*, Math. Comput., 35, (1991), pp. 773–782.
[34] O. Pironneau, *Optimal Shape Design for Elliptic Systems*, Springer Verlag, Berlin, 1984.
[35] R.-E. Plessix, Y.-H. De Roeck, and G. Chavent, *Waveform inversion of reflection seismic data for kinematic parameters by local optimization*, SIAM J. Sci. Comput., 20 (1999), pp. 1033–1052.
[36] C. Prada, F. Wu, and M. Fink, *The iterative time reversal mirror: A solution to self-focusing in the pulse echo mode*, J. Acoust. Soc. Amer., 90 (1991), pp. 1119–1129.
[37] J.-P. Puel and M. Yamamoto, *Generic well-posedness in a multidimensional hyperbolic inverse problem*, J. Inverse Ill-posed Problems, 5 (1997), pp. 55–83.
[38] Rakesh, *Reconstruction for an inverse problem for the wave equation with constant velocity*, Inverse Problems, 6 (1990), pp. 91–98.
[39] V. G. Romanov, *Inverse Problems of Mathematical Physics*, VNU Science Press, Ultrecht, The Netherlands, 1987.
[40] V. G. Romanov, *Problem of determining the speed of sound*, Sib. Math., 30 (1990), pp. 598–605 (English translation by Plenum).
[41] K. Shirota, *A numerical method for the problem of coefficient identification of the wave equation based on a local observation of the boundary*, Comm. Korean Math. Soc., 16 (2001), pp. 509–518.
[42] H. Sielschott, *Rückpropagationsverfahren für die Wellengleichung in bewegtem Medium (Back-propagation method for the wave equation in moving media)*, Ph.D. thesis, Mathematisch-Naturwissenschaftliche Fakultät, Universität Münster, Münster, Germany, 2000.
[43] U. Tautenhahn, *Tikhonov regularization for identification problems in differential equations*, in Parameter Identification and Inverse Problems in Hydrology, Geology and Ecology (Karlsruhe, 1995), Kluwer Academic Publishers, Dordrecht, The Netherlands, 1996, pp. 261–270.
[44] U. Tautenhahn and Q.-N. Jin, *Tikhonov regularization and a posteriori rules for solving nonlinear ill posed problems*, Inverse Problems, 19 (2003), pp. 1–21.
[45] A. N. Tikhonov and V. Y. Arsenin, *Solution of Ill-posed Problems*, Wiley, New York, 1977.
[46] V. H. Weston, *Invariant imbedding and wave splitting in* $\boldsymbol{R}^d$, Inverse Problems, 8 (1992), pp. 919–947.